Microwave Nanosecond Pulse Burnout Properties of GaAs MESFET's

JAMES J. WHALEN, MEMBER, IEEE, MARK C. CALCATERA, AND MARK L. THORN

Abstract—**Microwave nanosecond pulse burnout data have been measured at 9.3 GHz for three commercially available 1-μm gate MESFET's. Values for the incident pulse power required to cause burnout are concentrated in the ranges 4–10 W for 10-ns pulses, 12–25 W for 3-ns pulses, and 15–30 W for 1.5-ns pulses. The corresponding values for the absorbed microwave pulse energy required to cause burnout are concentrated in the ranges 0.3 to 0.6 ergs for 10-ns pulses, 0.2–0.4 ergs for 3-ns pulses, and 0.2–0.35 ergs for 1.5-ns pulses.**

Two dominant failure modes in overstressed MESFET's have been observed. One is a gate-to-source low-resistance path (5–25 Ω) which frequently is correlated with metal migration (mainly gold) from the source metallization to the gate metallization. This failure mode was dominant when MESFET's failed at lower power levels as at 10 ns. The other dominant failure mode is a reduction in I_{DSS} or a drain-to-source short which is correlated with massive damage in the channel region between the source and gate metallizations. This failure mode was dominant when MESFET's failed at high power levels as at 1.5 ns.

I. INTRODUCTION

LOW-NOISE GaAs Metal-Semiconductor Field-Effect Transistors (MESFET's) are being developed for use as RF-amplifier stages in microwave receivers. One important application for these RF-amplifier stages will be in transmit–receive radar systems which share a common antenna. Transmit–receive radar systems usually will include protection devices to limit the microwave power incident upon the GaAs MESFET. Since the protection devices cannot respond instantaneously, there is a short duration of time (usually a few nanoseconds) during which the protection devices cannot limit the microwave power incident upon the GaAs MESFET. During this time duration, the MESFET may be degraded or burned out. Thus the reliability of such radar systems will depend upon the burnout properties of the GaAs MESFET. Information currently available on this subject is limited [1]–[4]. For this reason an experimental investigation has been carried out to obtain X-band nanosecond pulse burnout data for GaAs MESFET's

This paper is organized in the following manner. In Section II the physical characteristics of the three commercial 1-μm gate GaAs MESFET's selected for the investigation are presented. The X-band high-power nanosecond pulse system used to overstress the MESFET's and the test procedures are described in Section III. The electrical characteristics, and scanning electron microscope (SEM) characteristics of overstressed MESFET's are presented in Sections IV and V. MESFET X-band nanosecond pulse burnout results are given in Section VI. Section VII is the conclusion.

Manuscript received May 27, 1979; revised September 4, 1979. This work was supported by the Air Force Avionics Laboratory, Wright-Patterson Air Force Base, Dayton, OH, under contract F 33615-77-C-2059.

J. J. Whalen is with the Department of Electrical Engineering, State University of New York at Buffalo, Amherst, NY 14226.

M. C. Calcatera is with the Air Force Avionics Laboratory, Wright-Patterson Air Force Base, Dayton, OH 45433.

M. L. Thorn was with the Department of Electrical Engineering, State University of New York at Buffalo, NY. He is now with the Hewlett-Packard Company, Santa Rosa, CA 95404.

II. MESFET CHARACTERISTICS

For the MESFET burnout investigation three commercially available GaAs MESFET's with 1-μm gate lengths were selected. Type-A MESFET has a Ti/Pt/Au (or Ti/Cr/Pt/Au) gate metallization. Types-B and -C MESFET's have Al-gate metallizations. Additional information on the MESFET structures is given in Table I and in Appendix I.

The GaAs MESFET dice were bonded using silver epoxy to 50-Ω impedance microstrip circuits, and 0.7-mil gold bond wires were attached using thermocompression bonding techniques. Next the dc–voltage characteristics and X-band s parameters were measured and compared to those given in manufacturers' data sheets. Then noise figure and small-signal power gain measurements were made. As shown in Fig. 1, microwave-matching networks called METCHIP's were used. METCHIP's are rectangular sections cut from highly polished microwave substrate material (dielectric constant = 9.6 and thickness = 0.6 mm) which was purchased with a 3.8-μm thick gold layer on both sides. The upper gold layer was removed, and the substrate material was cut into rectangular sections. Typical sizes were 1.5 mm × 1.5 mm, 2.0 mm × 2.0 mm, 2.5 mm × 2.5 mm, and 3.0 mm × 3.0 mm. When placed symmetrically over the center conductor of the 50-Ω impedance microstrip transmission line as shown in Fig. 1, the rectangular section (METCHIP) behaves as a section of low-impedance transmission line. Using METCHIP's for input and output matching, single-stage MESFET noise figures in the 3.0–4.5-dB range with associated power gains in the 5–10-dB range at 9.35 GHz were obtained for MESFET Types-A, -B, and -C.

III. EXPERIMENTAL PROCEDURES

The X-band high-power nanosecond pulses used to overstress the GaAs MESFET's were generated using the system shown in Fig. 2. The CW source was a Gunn diode which oscillated at 9.3 GHz. The diode modulator was a

0018-9480/79/1200-1026$00.75 ©1979 IEEE

TABLE I
MESFET PHYSICAL CHARACTERISTICS

Parameter	Type-A	Type-B	Type-C
Gate Metal.	Ti/Cr/Pt/Au	Al	Al
Gate Pad	Ti/Cr/Pt/Au	Al	Ti/Pt/Au
Source-Drain (Ohmic Contact)	Au-Ge/Ni/Au	In/Ge/Au	Au-Ge/Pt
Source-Drain (Pad Overlay)	Ti/Cr/Pt/Au	None	Ti/Pt/Au
Gate Length	1 micron	1 micron	1 micron
Number of Gates	1	2	2
Total Gate Width	500 μm	300 μm	300 μm
Channel Length	3.5 μm	5 μm	3 μm
Glassivation (Over Channel)	Yes	No	Yes

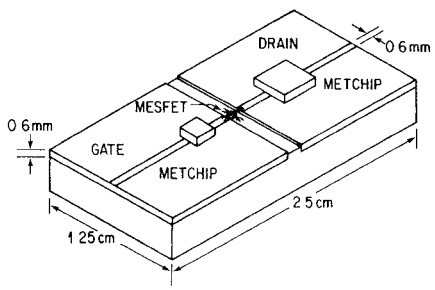

Fig. 1. *X*-band 50-Ω microstrip circuit illustrating locations of MESFET and METCHIP impedance transforming sections.

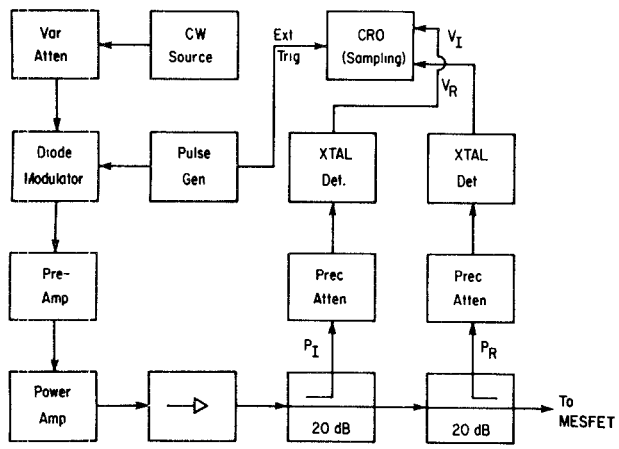

Fig. 2. *X*-band high-power nanosecond pulse system.

low-power switch that was turned on by a pulse from the pulse generator. When the pulse generator output voltage returned to zero, the diode switch returned to its normal (off) position. The diode switch output was a pulse amplitude modulated (PAM) *X*-band signal the envelope of which had a rise time of 1.5 ns and fall time of 2.0 ns. The diode switch PAM output was amplified by a wide-band low-power solid-state *X*-band preamplifier and by a wide-band high-power TWT amplifier with a maximum output power of 100 W. The *X*-band pulse power P_I incident upon a MESFET and power P_R reflected by a MESFET were measured using directional couplers and wide-band crystal detectors as shown in Fig. 2. The waveforms of the rectified voltage pulses at the crystal detector

TABLE II
X-BAND PULSE POWER TEST CONDITIONS

Frequency: 9.3 GHz

Pulse Duration: 1.5, 3.0 or 10 nsec

PRF: 10 kHz to 100 kHz

Exposure Time: 1 to 3 minutes

Sequence of Incidence Pulse Power Levels in Watts (1 dB Steps)

0.32	1.00	3.2	10.0	32
0.40	1.26	4.0	12.6	40[a]
0.50	1.58	5.0	15.8	50[a]
0.63	2.00	6.3	20.0	63[a]
0.79	2.51	7.9	25.1	

[a] Available but not used.

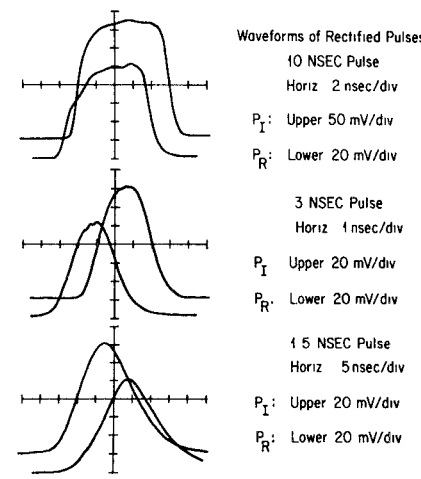

Fig. 3. CRO waveforms of rectified voltages corresponding to incident pulse power P_I and reflected pulse power P_R for pulse durations of 10, 3, and 1.5 ns.

outputs were displayed on a sampling CRO and photographed. Representative waveforms corresponding to pulse durations of 10, 3, and 1.5 ns are shown in Fig. 3. Using the calibration procedures described in Appendix II, the information contained in the rectified voltage pulse waveforms was processed to obtain values for the pulse power P_I incident upon the MESFET, the pulse power P_R reflected by the MESFET, and the pulse energy E_A absorbed by the MESFET.

After the GaAs MESFET noise figure and power gain were measured, it was exposed to an *X*-band pulse train for 1–3 min. The pulse duration was in the 1.5–10-ns range, and the pulse repetition frequency was in the 10–100-kHz range. The incident pulse (peak) power was set initially at 0.32 W. After the initial exposure of the GaAs MESFET to the *X*-band pulse train, the MESFET noise figure and power gain at 9.35 GHz were measured again. If no significant change in noise figure occurred, the incident pulse power was increased 1 dB and the MESFET was exposed again to an *X*-band pulse train. The procedure of increasing the incident pulse power in 1-dB steps was continued until a significant increase in MESFET noise figure was observed. The *X*-band high-power pulse conditions are summarized in Table II.

In almost every case no change in MESFET noise figure was observed until the incident pulse power was large enough to cause catastrophic failure. When catastrophic failure occurred, the total measurement system noise figure usually increased from 5 to 6 dB to more than 20 dB, and the small-signal power gain decreased to values less than 0.1. In addition abrupt changes in the dc drain and gate bias currents were observed. The changes in dc bias currents are described in the next section.

IV. Electrical Characteristics of Overstressed MESFET's

The dc–voltage characteristics of the overstressed MESFET's indicated two dominant failure modes. For a 10-ns pulse duration the dominant failure mode for all three MESFET types was a gate-to-source short-circuit. Typical values for the gate-to-source resistance were in the range 5–25 Ω. For a 3-ns pulse duration the dominant failure mode for Type-A and Type-C MESFET's was also a gate-to-source short-circuit, but the dominant failure mode for Type-B MESFET's was a reduction in the saturated drain current I_{DSS} measured at $V_{GS}=0$ V and $V_{DS}=2.5$ V. Typical values for I_{DSS} were in the range 0.1–10 mA. One Type-B MESFET exhibited an unstable I_D–V_{DS} characteristic which was essentially a drain-to-source short-circuit (17 Ω). Many Type-B MESFET's also exhibited a high resistance (>5 kΩ) path from gate-to-source. For a 1.5-ns pulse duration the dominant failure mode for all Type-A and some Type-B MESFET's was a reduction in I_{DSS} to values <1 mA. Also observed was a high resistance (>1 kΩ) path from gate-to-source. For some Type-B MESFET's the dominant failure mode was a low-resistance (20–50 Ω) gate-to-source short-circuit. For a 1.5-ns pulse duration the dominant failure mode for the Type-C MESFET's was a drain-to-source short-circuit (~5 Ω). Some Type-C MESFET's also exhibited an unstable I_D–V_{DS} characteristic. Also observed was a high-resistance path (>5 kΩ) from gate-to-source. In the next section the electrical characteristics of overstressed MESFET's will be related to damage observed using optical and scanning electron microscopy. (Additional information on the electrical characteristics of overstressed MESFET's is given in Appendix III.)

V. Optical and SEM Characteristics of Overstressed MESFET's

Prior to burnout photomicrographs of the channel region of each MESFET were made using an optical microscope. Following burnout, each MESFET was examined with an optical microscope (OM) and many were examined with a scanning electron microscope (SEM). Both OM and SEM photomicrographs were made of most overstressed MESFET's Also X-ray microanalysis was made on representative MESFET's to determine the atomic constituents in the materials in the damaged regions. This phase of the investigation is being continued.

Two dominant catastrophic failure modes have been identified using optical and scanning electron microscopy.

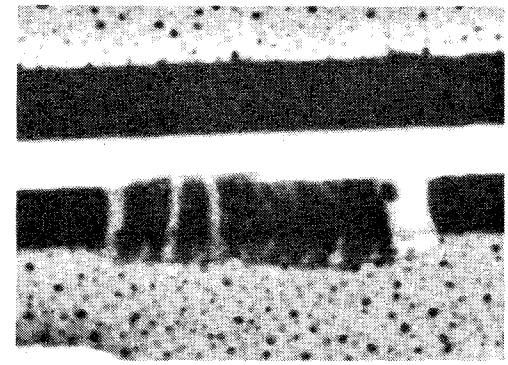

Fig. 4. SEM photomicrograph of Type-A MESFET overstressed with 10-ns pulse. The failure mode appears to be caused by metal migration of the source ohmic contact material (bottom) toward gate metallization (middle). The result is a gate-to-source short-circuit.

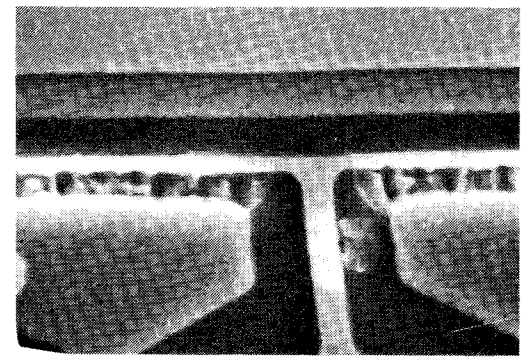

Fig. 5. SEM photomicrograph of Type-A MESFET overstressed with 1.5-ns pulse. The failure mode appears to be massive GaAs damage in the channel region between source (bottom) and gate (middle) metallizations. The result is a reduction in I_{DSS} to 0.1 mA.

These failure modes are called the metal migration (MM) mode and the massive channel damage (MCD) mode. For a 10-ns pulse duration the dominant failure mode for Types-A, -B, and -C MESFET's is MM which causes a gate-to-source low-resistance path. For a 1.5-ns pulse duration the dominant failure mode for Types-A, -B, and -C MESFET's is MCD which causes either a reduction in I_{DSS} values or an unstable low-resistance path from drain to source. These two failure modes will be illustrated using Type-A MESFET photomicrographs.

Shown in Fig. 4 is the damage caused by a 10-ns microwave pulse to a Type-A MESFET. The failure mode appears to be caused by MM of the source ohmic contact metal toward the gate metallization. The result is a low-resistance metallic bridge between source and gate metallizations. Point analysis and distribution mappings of the migrated metal clearly established the presence of gold—the main constituent in the ohmic contact metallization. Voiding of the source ohmic contact metal for a Type-A MESFET overstressed with 10-ns duration pulses is evident in Fig. 4. Photomicrographs for MESFET Types-B and -C are similar. Some voiding in the gold gate metallization also appears to exist in Fig. 4. Similar voiding in aluminum gate metallizations (Types-B and -C MESFET's) is not observed. Additional analysis is being conducted to determine the effects of a gold versus

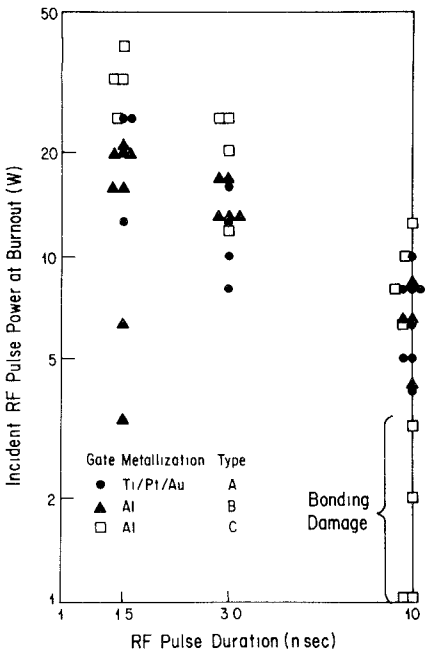

Fig. 6. Values of microwave incident pulse power P_I required to cause burnout versus pulse duration T. The P_I values are believed to be accurate ±0.5 dB.

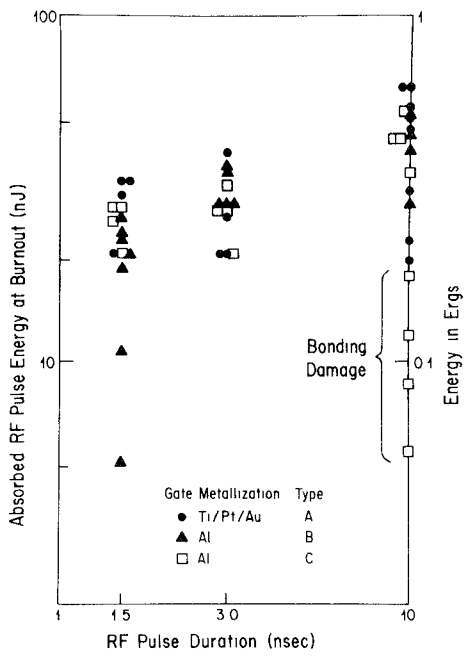

Fig. 7. Values of microwave absorbed pulse energy E_A required to cause burnout versus pulse duration T. The E_A values are believed to be accurate ±1.0 dB.

aluminum gate metallization upon the metal migration process. The dominant failure mode for Types-A and -C MESFET's overstressed with 3-ns microwave pulses is also the MM mode. However, another failure mode called the MCD mode did begin to manifest itself.

Shown in Fig. 5 is the damage caused by a 1.5-ns microwave pulse to a Type-A MESFET. The failure mode appears to be massive GaAs material damage in the channel region between the source and gate metallizations. The effect of the MCD for this MESFET was to reduce the I_{DSS} value to less than 0.1 mA and to cause a 3-kΩ resistance path between gate and source. The analysis of the material in the channel damage region is continuing. The channel damage failure mode was also the dominant failure mode for Types-B and -C MESFET's overstressed with 1.5-ns microwave pulses and for Type-B MESFET's overstressed with 3-ns microwave pulses.

VI. MESFET Nanosecond Burnout Results

Shown in Figs. 6 and 7 are the values of incident microwave pulse power P_I and absorbed microwave pulse energy E_A required to cause burnout for pulse durations of 1.5, 3, and 10 ns for the three MESFET types tested. The P_I values plotted in Fig. 6 are believed to be accurate to ±0.5 dB. The E_A values plotted in Fig. 7 are believed to be accurate to ±1.0 dB. (See Appendix II for a discussion of how values for P_I and E_A were determined.)

The data shown in Fig. 6 will now be discussed briefly. For a 10-ns pulse duration most P_I values lie in the 4–10-W range. Four Type-C MESFET's did fail at P_I values in the 1–3-W range, but these four MESFET's had suffered substantial damage during wire bonding. The gold metallization overlay on the source, gate, and drain pads were partially lifted when one or more wire bonds were attached. By modifying the wire-bonding technique, damage to Type-C MESFET's caused by the wire-bonding process was eliminated. For Type-C MESFET's the P_I values in the range 6–12 W and not the P_I values in the 1–3-W range are believed appropriate. However, it is thought worthwhile to include the burnout data for the MESFET's damaged during wire bonding because prior to burnout these MESFET's exhibited microwave performance comparable to MESFET's not damaged by the wire-bonding process. It may be concluded that although improper wire-bonding techniques may not always affect MESFET small signal microwave performance they can significantly lower the MESFET burnout pulse power level P_I. For a 3-ns pulse duration most P_I values lie in the 12–25-W range. Two Type-A MESFET's did fail at P_I values in the 8–10-W range, but both of these MESFET's had suffered some mechanical damage (cause unknown) to metallization areas prior to burnout. For a 1.5-ns pulse duration most P_I values lie in the 15–30-W range. Two Type-B MESFET's did fail at P_I values in the 3–6-W range. To date the cause for the lower P_I values has not been determined, and they are considered to be maverick MESFET's of considerable interest.

An attempt could be made to fit the P_I versus T data shown in Fig. 6 to a relationship

$$P_I(\mathrm{W}) = K_I[\,T\,(\mathrm{ns})\,]^n \qquad (1)$$

with $K_I = 25$ and $n = -0.5$. However, an exponent $n = -0.5$ is not consistent with the data shown in Fig. 7 for the absorbed microwave pulse energy E_A at burnout versus pulse duration. These data will now be discussed. For a 10-ns pulse duration most values for E_A lie in the range 30–60 nJ (0.3–0.6 ergs). The four Type-C MESFET's that failed with E_A values in the range 5–20 nJ were the MESFET's that suffered substantial damage

during wire bonding. For a 3-ns pulse duration most E_A values lie in the range 20–40 nJ (0.2–0.4 ergs). The two Type-A MESFET's with E_A values near 20 nJ were the MESFET's that suffered some mechanical damage; perhaps these E_A values should be weighted less than other E_A values. For a 1.5-ns pulse duration most E_A values lie in the range 20–35 nJ (0.2–0.35 ergs). The two Type-B MESFET's with E_A values in the 5–10-nJ range are the maverick MESFET's mentioned previously. If an attempt is made to fit the E_A versus T data to a relationship

$$E_A\,(\text{nJ}) = K_E[\,T\,(\text{ns})\,]^n \qquad (2)$$

the values $K_E = 22$ and $n = 0.3$ appear appropriate.

VII. Conclusion

Microwave nanosecond pulse burnout data have been measured at 9.3 GHz for three commercially available 1-μm gate MESFET's. The values for the incident pulse power required to cause burnout are concentrated in the ranges 4–10 W for 10-ns pulses, 12–25 W for 3-ns pulses, and 15–30 W for 1.5-ns pulses. The values for the absorbed microwave pulse energy required to cause burnout are concentrated in the ranges 0.3–0.6 ergs for 10 ns pulses, 0.2–0.4 ergs for 3-ns pulses, and 0.2–0.35 ergs for 1.5-ns pulses. MESFET's with Ti/Pt/Au (or Ti/Cr/Pt/Au) and Al gate metallizations appear to have similar burnout levels (within 2 dB).

Two dominant failure modes in overstressed MESFET's have been observed. One failure mode is a gate-to-source low-resistance path (5–25 Ω) which is correlated with MM (mainly gold) from the source metallization to the gate metallization. This failure mechanism was dominant in MESFET's overstressed with 10-ns pulses. The other dominant failure mode is a reduction in I_{DSS} or a drain–source short (usually unstable) which is correlated with massive GaAs material damage in the channel region between the source and gate metallizations. This failure mechanism was dominant in MESFET's overstressed with 1.5-ns pulses.

Appendix I
Additional MESFET Information

Shown in Figs. 8–10 are SEM photomicrographs for MESFET Types-A, -B, and -C which illustrate the layout of the source, gate, and drain regions and bonding pads. Also illustrated are the wire-bonding techniques. The information on the gate width, gate length, and channel length given in Table I may be used to estimate other MESFET dimensions. (Note that the width of each gate section of MESFET Type-B and Type-C is 150 μm.)

Appendix II
Determining Values for P_I and E_A

The procedures used to determine values for the incident microwave pulse power P_I and absorbed pulse energy E_A will be described briefly. Two crystal detectors were used to monitor the microwave pulse power incident

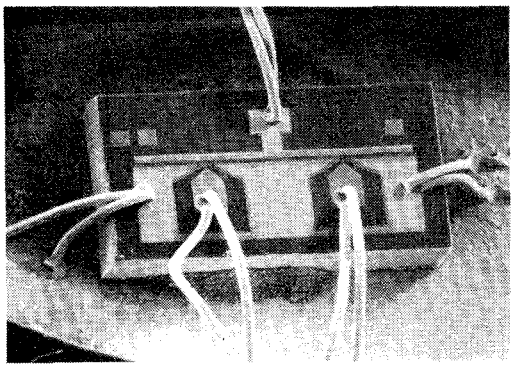

Fig. 8. SEM photomicrograph of Type-A MESFET illustrating physical features and wire bonds. The gate dimensions are 1 μm × 500 μm.

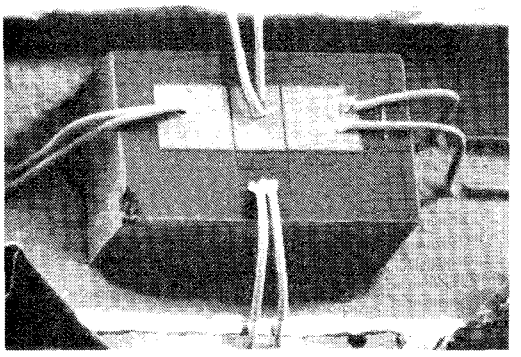

Fig. 9. SEM photomicrograph of Type-B MESFET illustrating physical features and wire bonds. The dimensions of each gate are 1 μm × 150 μm.

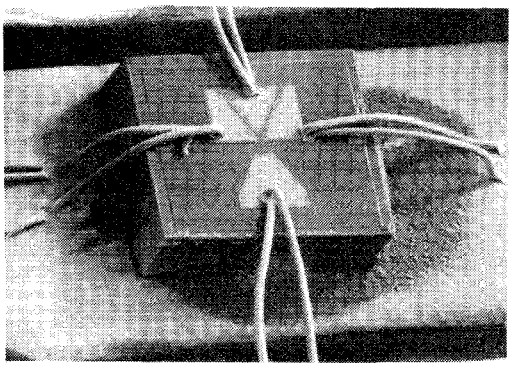

Fig. 10. SEM photomicrograph of Type-C MESFET illustrating physical features and wire bonds. The dimensions of each gate are 1 μm × 150 μm.

(P_I) upon a MESFET and reflected (P_R) from a MESFET. Shown in Fig. 3 are representative waveforms of the rectified pulses observed on a sampling CRO. The rectified voltage observed on the CRO was related to the microwave power incident upon the crystal detector via a calibration curve. The calibration curve was established by measuring for each crystal detector the dc-rectified voltage produced by a CW (sinusoidal) microwave signal. The waveforms of rectified voltage versus time shown in Fig. 3 were converted to waveforms of microwave power versus time. Using a trapezoidal integration procedure, the area under the converted waveform of microwave power versus time was calculated to obtain values for the incident pulse energy E_I and reflected pulse energy E_R. The absorbed pulse energy E_A was calculated using the

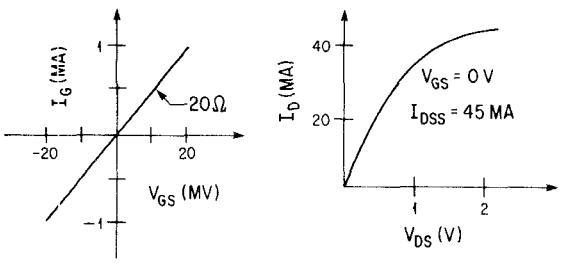

(a) (b)

Fig. 11. Overstressed MESFET I–V characteristics for the gate–source short-circuit failure mode. (a) Gate–source short circuit. (b) Normal I_D–V_{DS} characteristics.

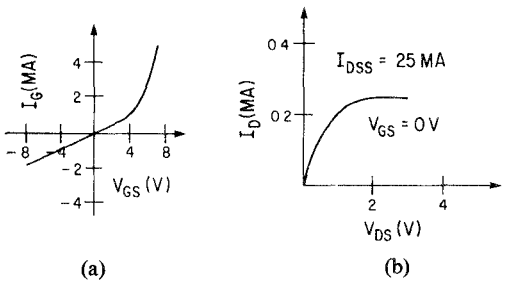

(a) (b)

Fig. 12. Overstressed MESFET I–V characteristics for the drain current reduction failure mode which corresponds to massive GaAs damage in the channel. (a) 4-kΩ gate–source short-circuit. (b) I_{DSS} reduction.

expression

$$E_A = E_I - E_R. \tag{II-1}$$

In using (II-1) to calculate values for E_A, the assumption is being made that the pulse energy E_T transmitted through the MESFET is negligible. The values calculated for E_I and E_R are thought to be accurate to ±10 percent (0.5 dB). Since values for the ratio E_R/E_I were usually less than 0.5 (even at high-power levels), the values for E_A obtained using (II-1), are thought to be accurate to ±25 percent (1 dB).

Appendix III
I–V Curves of Overstressed MESFET's

Shown in Fig. 11 are gate–source and drain–source current–voltage characteristics of an overstressed MESFET which illustrate the gate-to-source short-circuit failure mode. The I_G–V_{GS} characteristic corresponds to a 20-Ω resistor. The I_D–V_{DS} characteristic corresponds to the normal MESFET drain characteristic with V_{GS}=0 V. Optical and SEM photomicrographs clearly showed a metallic bridge between source and gate metallizations similar to that shown in Fig. 4.

Shown in Fig. 12 are the gate–source and drain–source current–voltage characteristics of an overstressed MESFET which illustrates the drain current reduction failure mode. The I_G–V_{GS} characteristic corresponds to that of a Schottky barrier diode shunted by a 4-kΩ resistor. The I_D–V_{DS} characteristic corresponds to that of a MESFET with a very low I_{DSS} value (0.25 mA). Optical and SEM photomicrographs indicated massive damage to the GaAs material in the channel region between source and gate metallizations similar to that shown in Fig. 5.

References

[1] D. A. Abbott and J. A. Turner, "Some aspects of GaAs FET reliability," *IEEE Trans. Microwave Theory Tech.*, vol. MTT-24, pp. 317–321, June 1976.

[2] R. F. Haythronthwaite, S. P. Bellier, and J. L. May, "Reliability studies of gallium arsenide field effect transistors using a scanning electron microscope," Dep. Commun., Commun. Res. Centre, Ottawa, Canada.

[3] R. Lundgren, "Reliability study of GaAs FET," Rome Air Development Center, Griffiss Air Force Base, NY Tech. Rep. RADC-TR-78-213, Oct. 1978.

[4] R. E. Lundgren and G. O. Ladd, "Reliability study of microwave GaAs field-effect transistors," 1978 Int. Reliability Physics Symp., (San Diego, CA), Apr. 18–20, 1978, in *Proc. 16th Ann. Reliability Physics*, 1978.